Biocompatible Lipid-Based Liquid Crystals and Emulsions

Monica Mosca,[†] Sergio Murgia,[‡] Andrea Ceglie,[†] Maura Monduzzi,[‡] and Luigi Ambrosone*[,†]

Department of Food Technology, Università del Molise, via De Sanctis, I-86100 Campobasso (CB), Italy, and Department of Chemical Science, Università di Cagliari, s.s. 554 Bivio Sestu, 09042 Monserrato (CA), Italy

Received: April 28, 2006; In Final Form: September 29, 2006

Due to its potential relevance as a fully biocompatible formulation useful in cosmetic, food, and pharmaceutical applications, the glycerol trioleate/sodium oleate/water ternary system was investigated via optical microscopy and NMR methods. The ternary diagram is dominated by monophasic and biphasic regions where a lamellar phase coexists with different isotropic phases. A broad emulsion region, characterized by small oil droplets dispersed within the lamellar phase, extends from the center toward the water corner of the diagram. Information on the inner structure of these emulsion-like samples is supplied by modeling water and oil NMR self-diffusion data. Sizing of oil droplets was provided at different storage times. A highly polydisperse log-normal distribution was observed. The presence of the liquid crystalline phase is called into play for the negligible differences found in the droplets size distribution upon samples aging. Indeed, samples within this region stored at 25 °C did not show phase separation after several months from their preparation.

1. Introduction

As a consequence of their amphiphilic nature, polar lipids may self-assemble into a variety of aggregates having normal or reversed curvature ranging from dispersed micellar, cubic, and hexagonal to lamellar phases. Among the others, binary and ternary or pseudo-ternary systems based on esterified polyalcohols, such as mono- and diglycerides and esters of polyglycerols, have been extensively studied in the past decade. Due to the rich polymorphism they exhibit along with the possibility to adjust their physicochemical properties (i.e., charge, size of the aqueous cavities) these systems have been proposed as suitable candidates mainly for pharmaceutical formulations useful in controlled drug release.[1] The rationale behind these investigations is to offer an answer to the manufacturers increasing demand for delivery systems able not only to host sparingly soluble therapeutic agents but to improve the therapeutic performance of the drug as well. An emblematic case is given by liposome architectures that allow the therapeutic properties of the drug to be expressed with improved pharmacokinetics, enhanced efficacy, and reduced toxicity. Moreover, since the early 1960s lipid based emulsions have been used as a base for both oral and injectable formulations, as solubility enhancers or to improve pharmacokinetics properties. Initially developed as a safe parenteral product for clinical nutrition (Intralipid), fat emulsions rapidly disclosed their ability as drug carriers leading to commercial products of considerable success. Diazemuls (used for sedation) and Diprivan (induction and maintenance of anesthesia) are significant examples.[2]

In this context, and to evaluate the potential of liquid crystals in stabilizing emulsions for drug delivery, several monoolein based pseudo-ternary systems were recently explored.[3,4] All of the systems are characterized by a narrow reverse microemulsion region along with a biphasic liquid crystalline region (lamellar and reverse hexagonal) that, upon water swelling, becomes the matrix into which excess of water can be dispersed as small droplets. Such emulsions are endowed with a long shelf life while the method of preparation is pointed out as a critical stage.

Under the same perspective, the phase behavior of the ternary system glycerol trioleate/sodium oleate/water (GTO/NaO/W) is here investigated by means of optical microscopy and nuclear magnetic resonance techniques. Results will provide further understanding of the phase behavior of lipid and surfactants which are found as ingredients of pharmaceutical products. In addition, the wide oil in liquid crystalline stabilized emulsion area that dominates the ternary diagram would be suitable to solubilize water-insoluble moieties.[5]

2. Materials and Methods

Materials. Glycerol trioleate (GTO), with a purity of 65 wt %, was purchased from Sigma. A careful investigation via quantitative proton-decoupled ^{13}C NMR provided the complete glycerides composition (results are expressed as mol %): triglycerides = 73.3; 1,3-diglycerides = 16.6; 1,2-diglycerides = 7.2; monoglycerides = 2.9; impurities = 1.0. Concerning the acyl side-chains, an oleic/linoleic = 90.3/9.7 molar ratio was detected.

Sodium oleate (NaO) was from J. T. Baker. Distilled water (W) passed through a Milli-Q water purification system (Millipore) was used to prepare the samples for the ternary diagram determination. When required (see below) samples were prepared using deuterated water from Fluka.

Sample Preparation. Samples of about 2000 mg in size were prepared by gradual addition of water to the GTO/NaO binary mixture up to the desired composition in sample tubes (∅ =1.5 cm) that were subsequently sealed by screw plugs. Then, samples were thoroughly mixed by means of a Vortex mixer (IKA MS2) used at 2500 rpm until they appeared to be homogeneous. Finally, samples were left to equilibrate at 25 °C for one week before any measurement was taken. The observation of the macroscopic properties of the sample (phase number, physical state, homogeneity, and birefringence) by visual inspection and optical microscopy at 25 °C allowed a

* To whom correspondence should be addressed. Phone: +39 0874 404715. E-mail: ambroson@unimol.it.
[†] Università del Molise.
[‡] Università di Cagliari.

10.1021/jp062622y CCC: $33.50
Published on Web 11/30/2006

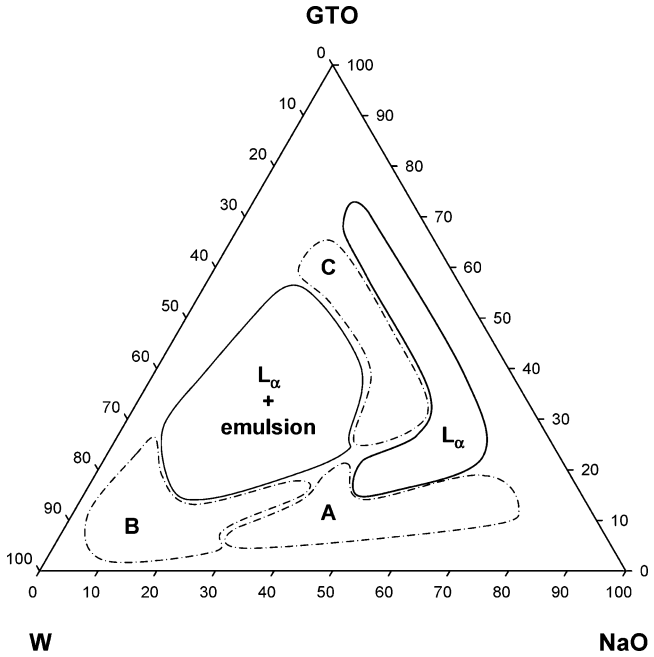

Figure 1. Schematic GTO/NaO/W ternary diagram at 25 °C. Dash-dotted boundaries delineate biphasic regions whose description is given in the text. Axes units are in wt %.

preliminary diagram characterization. Throughout the paper, except otherwise stated, the samples composition will be given as weight percent.

Optical Microscopy. Information about the droplet size distributions of samples from the "L_α + emulsion" region (see Figure 1) were obtained by means of an optical microscope (Zeiss Axioplan 2) connected to a video camera, at 25 °C. In order to get representative results from the microscopic analysis of the emulsions, the Video Enhanced Microscopy technique was used. Such a technique combines the magnification power of a microscope with the digital image acquisition capability of a video camera. A series of images for each sample (9−10 pictures, 1000 objects) was analyzed to extract the droplets size polydispersity, which was estimated by counting the droplet "average number" at the different radii in micrographs of a Thoma grating. Image analysis software (Sigma Scan Pro, SPSS Science Software products), which provides a wide range of analytical features in addition to image enhancement, was used for digitizing the images. Moreover, since the emulsion droplets size distribution strongly depends on the energy input used during preparation, emulsion samples were all homogenized for the same time (15 min) as previously described. To identify anisotropic phases, samples were observed by the same device as indicated above in polarized light at 25 °C. The presence and the kind of liquid crystalline phases were characterized on the basis of the observed textures.[6]

Nuclear Magnetic Resonance (NMR). ^{1}H, ^{2}H, and ^{23}Na NMR measurements were carried out through a Bruker Avance 300 MHz (7.05 T) spectrometer at the operating frequencies of 300.131, 46.072, and 79.390 MHz, respectively, at 25 °C. A standard variable temperature control unit (with an accuracy of ± 0.5 °C) was used.

^{23}Na NMR Quadrupolar Splittings. Nuclei with spin $I \geq 1$ possess a quadrupole moment that interacts with the electric field gradient generated by the surroundings charge distribution. In an isotropic environment, molecular motion will average out the quadrupole coupling, while in highly ordered systems, this interaction will split in $2I$ peaks the otherwise single resonance. In anisotropic systems like lamellar liquid crystalline phases, the sodium ions resonance (and similarly for all nuclei with $I = 3/2$) will result in a central line flanked by two satellites. For powder samples (characterized by randomly oriented micro-domains), assuming a two site model with a fast chemical exchange between bulk ions (isotropic setting) and bound ions residing at the interface, the quadrupolar splitting $\Delta\nu_q$, measured as the distance between the central line and the satellites, will be given by[7,8]

$$\Delta\nu_q = |\sum_i p_b^i \nu_q^i S_b^i| \quad (1)$$

Here, considering the possible existence of different bound sites (i), the observed splitting is assumed to be an average over all of the sites, where $\nu_q = e^2qQ/4h$ represents the effective quadrupolar coupling constant, $S_b = 1/2(3\cos^2\theta - 1)$ is the order parameter related to the average time orientation of the nucleus with respect to the interface symmetry axis, and p_b is the fraction of nuclei in the bound state.

Each sample was left for 30 min in the NMR probe to ensure thermal equilibrium and alignment in the magnetic field before recording the spectra at 25 °C. The error in the quadrupole splitting measurements was always less than 4%.

Self-Diffusion Experiments. Monitoring the molecular diffusion via the pulsed field gradient spin−echo (PGSE) NMR technique benefits from certain advantages. Among the others, this technique is capable of measuring self-diffusion coefficients over a wide range from fast (above 10^{-9} m^2 s^{-1}) to very slow diffusion (below 10^{-14} m^2 s^{-1}) and can provide individual self-diffusion coefficients from mixtures without the need of artificial labeling. Self-diffusion measurements were here performed using a Bruker DIFF30 probe equipped with specific inserts for ^{1}H and ^{2}H nuclei and supplied by a Bruker Great 1/40 amplifier that can generate field gradients up to 1200 G cm^{-1}. The measurements were performed at (25 ± 0.5) °C by using the stimulated echo sequence (PGSTE) rather than the classical Hahn echo. Indeed, the study of emulsion systems often requires measurements at different diffusion times Δ. However, varying Δ in classic spin−echo experiments gives a strong dependence on the spin−spin relaxation time (T_2). Particularly, in emulsion systems, T_2 can be dominated by slow overall dynamics so that varying Δ in the Hahn echo pulse sequence may produce an unwanted size selection.[9] On the other hand, varying Δ in PGSTE experiments provides results which depend on spin−lattice relaxation time (T_1). Since T_1 at the applied field depends only on the short scale (∼nm) structure, no selection on the basis of the large structure can be expected. In other words, PGSTE measurements performed at different Δ show the real diffusion effect (e.g., effect due to molecular exchange) free from relaxation artifacts.

Using the common Stejskal−Tanner pulse sequence with two gradient pulses of duration δ, separation Δ, and strength g, the echo decay E in the NMR experiment is given by

$$\ln(E/E_0) = -(\gamma g\delta)^2 D t_D = -q^2 D t_D \quad (2)$$

where $t_D = (\Delta - \delta/3)$ is the diffusion time and the coefficient $q = \gamma g\delta$ represents the so-called "scattering vector". It should be noticed that, within the narrow-pulse limit ($\delta \rightarrow 0$), where the diffusion time t_D approximates the gradient separation Δ, t_D, and Δ can be used synonymously.[10] The echo attenuations were measured by recording the signal intensity in both the ^{1}H and ^{2}H NMR spectra, obtained by Fourier transform of the second half of the echo. Experiments were carried out by varying the magnitude of the applied magnetic field gradient g while

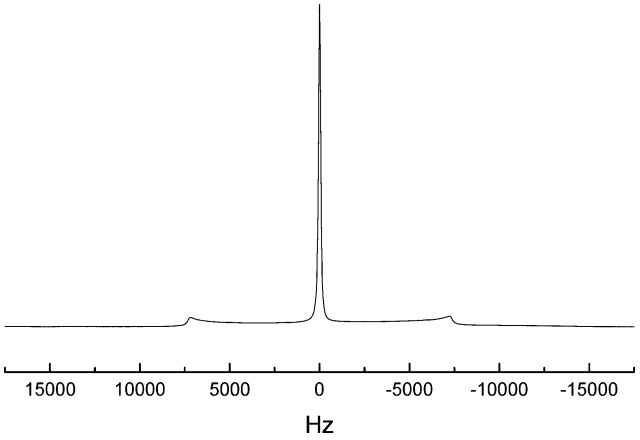

Figure 2. ^{23}Na NMR powder spectra of a L_α phase sample of composition GTO/NaO/W = 21/49/30.

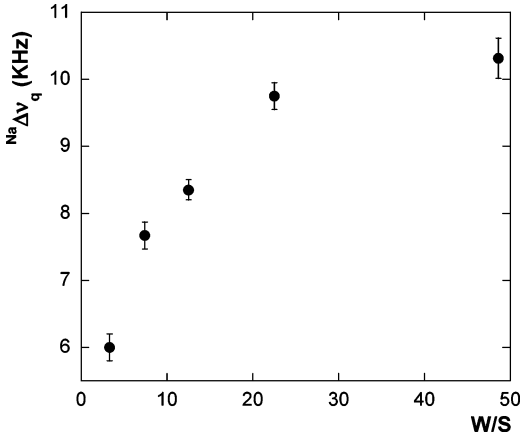

Figure 3. ^{23}Na NMR quadrupolar splittings measured upon water swelling along the GTO/NaO = 50/50 dilution line in the GTO/NaO/W system (W/S = water to sodium oleate molar ratio).

keeping δ and Δ constant during each experimental run. If the process underlying the molecular diffusion is typically Gaussian (free diffusion), eq 2 predicts that the self-diffusion coefficient D can be extracted from the slopes of the attenuation profiles obtained from linear regression of $\ln(E/E_0)$ as a function of q^2t_D at fixed δ and t_D. Conversely, if diffusion takes place within a confined geometry, deviation from linearity and a time (Δ) dependent behavior of the echo decay are both expected (restricted diffusion). All samples were prepared in duplicate, and all measurements were carried out in triplicate. The reproducibility, as estimated from repeated measurements, was evaluated within 7%.

3. Results and Discussion

Phase Behavior. Before starting the description of the GTO/NaO/W ternary diagram, some considerations on the "real" samples composition have to be made. As revealed by a quantitative proton-decoupled ^{13}C NMR analysis, GTO used in this work is, indeed, a mixture of oleic and linoleic triglycerides, containing more than 26 mol % of mono- and diglycerides (see Materials and Methods section). Clearly, synergism between the partially esterified glycerol molecules and the anionic sodium oleate (which forms mixed aggregates)[11] ought to be accounted for by the variety of structural morphologies shown by this system (and whose existence could hardly be attributable to the pure glycerol trioleate). Thus, because of the central role played by the GTO "impurities", what we will continue to refer to as a ternary diagram should be essentially considered as a multicomponent system.

The GTO/NaO/W ternary diagram at 25 °C is reported in Figure 1 (errors in phase boundaries determination are within ± 3 wt %).

The ternary diagram is dominated by a narrow liquid crystalline (LC) lamellar phase (L_α) region that borders the GTO/NaO binary axis, along with a broad LC-stabilized emulsion region that extends from the center of the diagram toward the water corner. All over the diagram, the nature of LC phases was established by combining optical microscopy in polarized light and ^{23}Na NMR quadrupolar splitting measurements. In Figure 2, the typical ^{23}Na NMR powder spectra of a sample with composition GTO/NaO/W = 21/49/30 is shown. Particularly, it has been observed that the ^{23}Na NMR quadrupolar splittings ($^{Na}\Delta\nu_q$) magnitude increases upon water addition, as shown in Figure 3. Actually, this behavior is not unusual in lyotropic LC phases. It has been earlier proposed to take place because of a change in the average order parameter (S_b) determined by a variation in the effective angle between the interface symmetry axis and the electric field gradient at the nuclei (θ) in the different sites i (see eq 1).[12]

Turning our attention to the ternary diagram, below the GTO/NaO = 25/75 weight ratio and up to about 65 wt % of water only a biphasic region exists (A region in Figure 1). Here, a L_α phase works as a dispersion matrix for undefined very small particles (diameter around 1 μm). In Figure 4a, a micrograph obtained from a sample with composition GTO/NaO/W = 10/54/36 shows the maltese crosses pattern characteristic for a L_α phase containing liposomes. For further water addition, samples belonging to this region show phase separation after centrifugation (3000 rpm for 15 min). An upper L_α phase and an isotropic pale-yellow lower solution were recovered.

Finally, at higher water content, samples evolve toward a wide biphasic region located at the water corner of the ternary diagram (B region in Figure 1).

Here, gravitational separation rapidly leads to a creamy phase (that does not show any birefringence) on the top and to a turbid solution that becomes bluish as the water content increases on the bottom of the sample tube. The occurrence of a liposomal dispersion may be suggested on the basis of the visual inspection of the lower phase.[13]

A monophasic lamellar LC region forms close to the GTO/NaO binary axis for GTO content between 20 and 75 wt %. This LC region extends from a minimum of 9 wt % up to about 38 wt % of water. Taking into consideration the high percentage of diglycerides in the GTO mixture, the existence of the L_α phase was expected. Indeed, these molecules are characterized by a high surface activity and are well-known as lamellar phase forming species because of their peculiar molecular shape.[4,14,15]

Upon water addition and for a GTO/NaO ratio between 80/20 and 28/72, the system enters a biphasic region where excess oil (that separates on the top of the samples after centrifugation) coexists with the L_α LC phase (C region in Figure 1). Nevertheless, increasing the water content further and provided that adequate energy is supplied during sample preparation (see the Materials and Methods section), the excess of oil can be incorporated within the LC matrix as a fine dispersion of small droplets. The system evolves into a kinetically stable emulsion region that extends up to about 70 wt % of water. It may be suggested that in this region water swells the L_α phase so that it can reach the necessary fluidity to operate as a very effective dispersing medium.

Emulsion Region. The emulsion-like structure of samples in such a region is clearly identified through optical microscopy

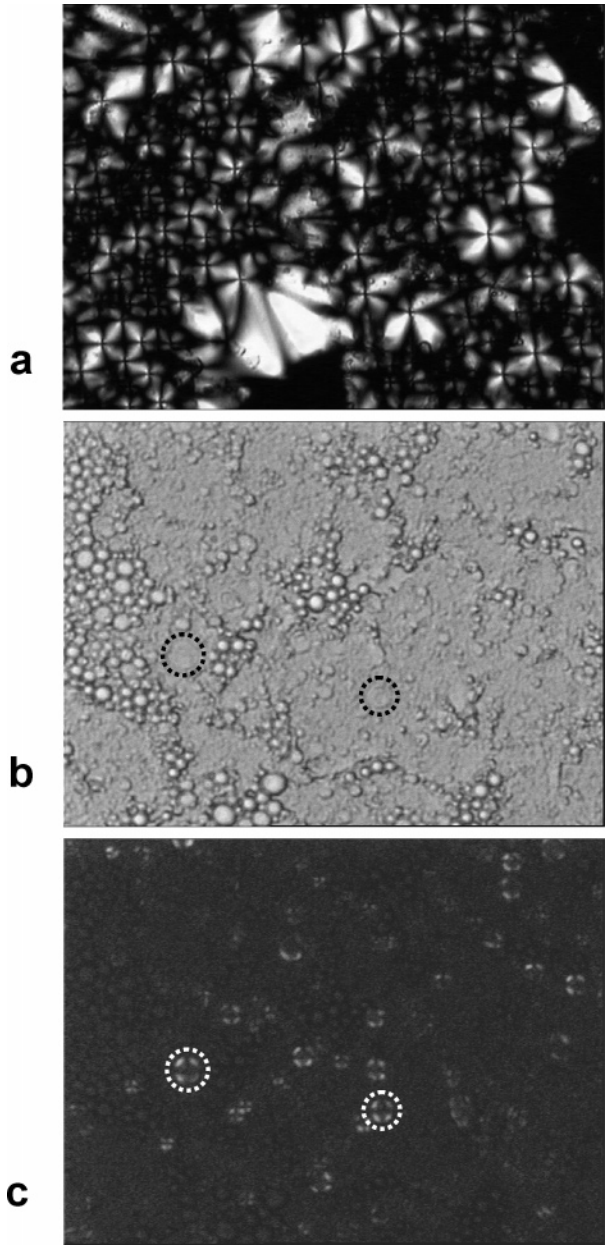

Figure 4. Micrographs recorded in polarized and normal light representative of the GTO/NaO/W ternary diagram (magnification 320×): (a) strongly birefringent maltese crosses and small particle dispersion in the sample with GTO/NaO/W = 10/54/36 composition (within the A region in Figure 1); (b) emulsion-like structure and (c) maltese crosses in a sample of GTO/NaO/W = 30/30/40 composition. Micrographs b and c belong to the same optical field, and circles provide a guide for the eyes to spot some liposomes.

(see Figure 4b). Both optical microscopy in polarized light (see Figure 4c) and ^{23}Na NMR experiments (see Figures 2 and 3) confirm the presence of the L_α LC phase as dispersing medium.

Oil Droplets Size Distribution. The oil droplet size distributions of two samples located within the emulsion region and having composition GTO/NaO/W = 30/30/40 (S1) and GTO/NaO/W = 20/20/60 (S2) were obtained via video enhanced microscopy (VEM) technique. Generally, the experimental results are well described by a log-normal distribution

$$P(R) = \frac{1}{\sqrt{2\pi\sigma^2}R}\exp\left[-\frac{(\ln R - \ln R_0)^2}{2\sigma^2}\right] \qquad (3)$$

that depends on the geometric mean R_0 and on the geometric

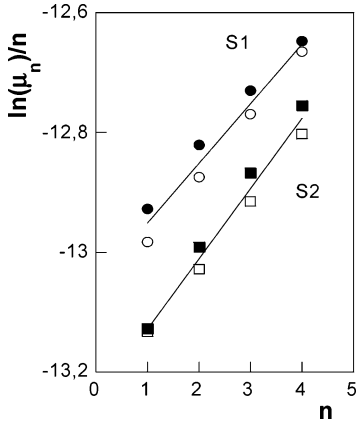

Figure 5. Assessment of the log-normal distribution for samples S1 (GTO/NaO/W = 30/30/40) and S2 (GTO/NaO/W = 20/20/60) at different storage times (open symbols: $t = 0$, filled symbols: $t = 3$ weeks) obtained through the VEM technique.

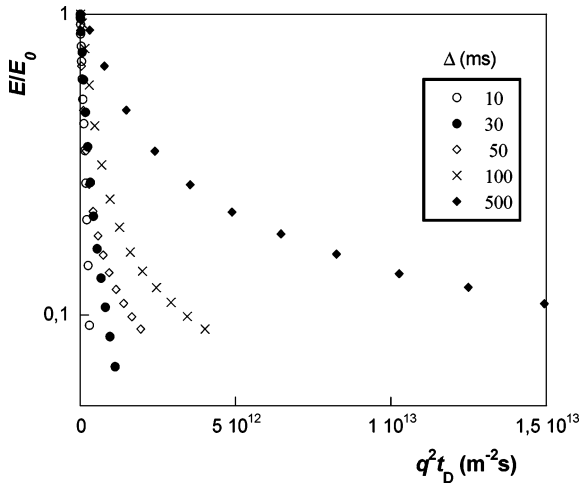

Figure 6. Semilog plot of the experimental GTO oil echo decay vs q^2t_D at different Δ values (sample composition: GTO/NaO/W = 30/30/40).

TABLE 1: Results of the VEM Size Distribution Determinations Concerning Two Emulsion Samples Differing in Water Content

sample	$R_0 \times 10^6$ (m)	σ^2
S1: GTO/NaO/W = 30/30/40	2.14 ± 0.05	0.20 ± 0.01
S2: GTO/NaO/W = 20/20/60	1.77 ± 0.03	0.23 ± 0.02

variance σ^2 of the distribution. Since for such a distribution the nth moment is given by[16]

$$\mu_n = R_0^n \exp(n^2\sigma^2/2) \qquad (4)$$

R_0 and σ^2 can be directly calculated through a linear regression of a plot of $\ln[\mu_n]^{1/n}$ versus n (Figure 5). Results are presented in Table 1.

Independently of the water content, both freshly prepared and aged (three weeks storage) emulsions display the same linear trend. Therefore, it can be inferred that these systems are kinetically stable and can be described with a log-normal distribution.

Oil Self-Diffusion. Figure 6 shows the semilog plot of the experimental echo decay, obtained for the GTO oil ^{1}H NMR signal, versus q^2t_D of a sample with composition GTO/NaO/W = 30/30/40. Deviations from normal Gaussian behavior are clearly suggested by (a) deviations from linearity of the

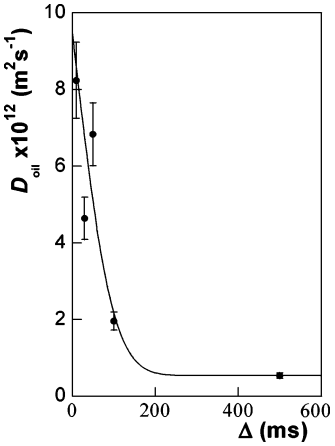

Figure 7. Oil self-diffusion coefficient (D_{oil}) at different experimental times (Δ).

monoexponential echo decay and (b) time dependence of the self-diffusion coefficient. These observations indicate that the oil molecules diffuse within limited volumes.

The echo amplitude in the case of unconstrained diffusion (e.g., Fick diffusion of molecules in isotropic bulk liquid) is described by eq 2. On the other hand, the translational motion in heterogeneous systems is strongly affected by the internal structure of the sample and typically appears dependent on the observation time. Here, from diffusion measurements at different t_D times, $D(t)$ coefficients are calculated using a linear regression of eq 2 applied only to the lowest q^2t_D values.[10] This procedure was repeated for values of Δ ranging from 30 to 500 ms. Results are plotted in Figure 7.

The best fitting of these data shows that, within 5% of error, the time dependence of $D(t)$ is well represented by

$$D(t) = A + B\ \mathrm{erfc}(t/\tau) \tag{5}$$

where erfc(x) is the complementary error function and A, B, and τ are the fitting parameters. Particularly $A = (0.05 \pm 0.01) \times 10^{-11}$ m^2 s^{-1}, $B = (0.9 \pm 0.1) \times 10^{-11}$ m^2 s^{-1}, and $\tau = (0.11 \pm 0.03)$ s are the calculated parameters in the present case. This experimental evidence can be physically rationalized as follows. If a domain volume is given by L^3, the distribution of domain sizes can be characterized by a normalized function $\rho(L)$ such that $\rho(L)L^2\,\mathrm{d}L$ represents the probability of finding a molecule in a domain of size between L and $L + \mathrm{d}L$. The measured self-diffusion coefficient involves the motion of molecules over many domains. This leads to an average over the distribution $\rho(L)$, i.e.

$$D(t) = \int_0^\infty L^2\rho(L)D(L,t)\,\mathrm{d}L \tag{6}$$

where $D(L,t)$ is the local diffusion coefficient at the time t in the domain of size L.

The structural properties of a fluid system are determined by the nature of the molecular motions in the fluid. These motions may be characterized by a number of properly chosen time correlation functions. Therefore, it is convenient to define the short-time and long-time diffusion coefficients as

$$D(0) = \int_0^\infty L^2\rho(L)D(L,0)\,\mathrm{d}L \text{ and } D(\infty) = \int_0^\infty L^2\rho(L)D(L,\infty)\,\mathrm{d}L \tag{7}$$

The experimental diffusion coefficient can be written as a superposition of the short-time and long-time limits of the diffusion coefficients

$$D(t) = D(\infty) + [D(0) - D(\infty)]\Gamma(t) \tag{8}$$

where

$$\Gamma(t) = \frac{1}{[D(0) - D(\infty)]}\int_0^\infty L^2\rho(L)[D(L,t) - D(L,\infty)]\,\mathrm{d}L \tag{9}$$

On the basis of eqs 6 and 7 it results $\Gamma(0) = 1$ and $\Gamma(\infty) = 0$.

Combining eqs 5 and 8 $D(\infty) = A$ and $D(0) = A + B$ can be deduced. In addition, it should be noticed that the empirical value of $D(0) = 0.95 \times 10^{-11}$ m^2 s^{-1} is very close to $D_{oil} = 1.00 \times 10^{-11}$ m^2 s^{-1} measured in our pure GTO.

According to the Felderhof's theory,[17] the term $[D(0) - D(\infty)]\Gamma(t)$ is related to the memory function through the relationship

$$\Gamma(t) = -[D(0) - D(\infty)]\int_t^\infty M(0,t')\,\mathrm{d}t' \tag{10}$$

where $M(0,t)$ is the memory function at zero wave number.

Then, the experimental results show that $\Gamma(t) = \mathrm{erfc}(t/\tau)$; that is, the memory function has a Gaussian form. The time scale characterizing the rate of change of the memory function is defined by

$$\tau_M = \int_0^\infty \Gamma(t')\,\mathrm{d}t' = \tau/\sqrt{\pi} = 0.06\ \mathrm{s} \tag{11}$$

Within the formalism of this model, $D(L,t)$ changes only at the domain boundaries, and $\tau_M \approx L^2/D(0) = 0.4$ s can be obtained using the data of Table 1. It is worth noticing that this value differs less than 1 order of magnitude with respect to that calculated in eq 11. This means that most oil molecules are forced to diffuse within spherical domains.

Water Self-Diffusion. As previously observed, samples within the emulsion region look like a coarse dispersion of both oil droplets and onion-like liposomes particles (see Figure 4b,c). Taking into account the heterogeneity of this system, modeling water self-diffusion data appears to be a quite complicated task. Indeed, water translational motion will be strongly influenced by the different kinds of domains where such molecules diffuse. Basically, obstructed diffusion for molecules outside the liposomes as well restricted diffusion for molecules confined inside the liposomes should both contribute to the echo decay in the PGSTE experiment. In addition, due to eventual defects in the liposomes bilayer, water molecules might diffuse across the layers thus complicating further the NMR results. Nevertheless, qualitative information about the sample inner structure can still be obtained.

To avoid radiation damping artifacts while measuring water self-diffusion, the samples S1 and S2 were both prepared using deuterated rather than distilled water. Figure 8a,b shows the water NMR echo decay vs q^2t_D of these samples, measured at different Δ values, as detected through the ^{2}H PGSTE experiment. It can be observed that such data, particularly those concerning the sample with the higher water content (S2), reveal only a very small dependence on Δ.

This result may be explained considering that most water diffuses outside the liposomes. Therefore, water trapped inside the liposomes and undergoing the restricted diffusion regime contributes only slightly to the NMR signal decay. It should also be noticed that, as a general rule, the signal attenuation caused by molecule diffusive motions within barriers becomes constant for a sufficiently long diffusion time t_D. Since this effect

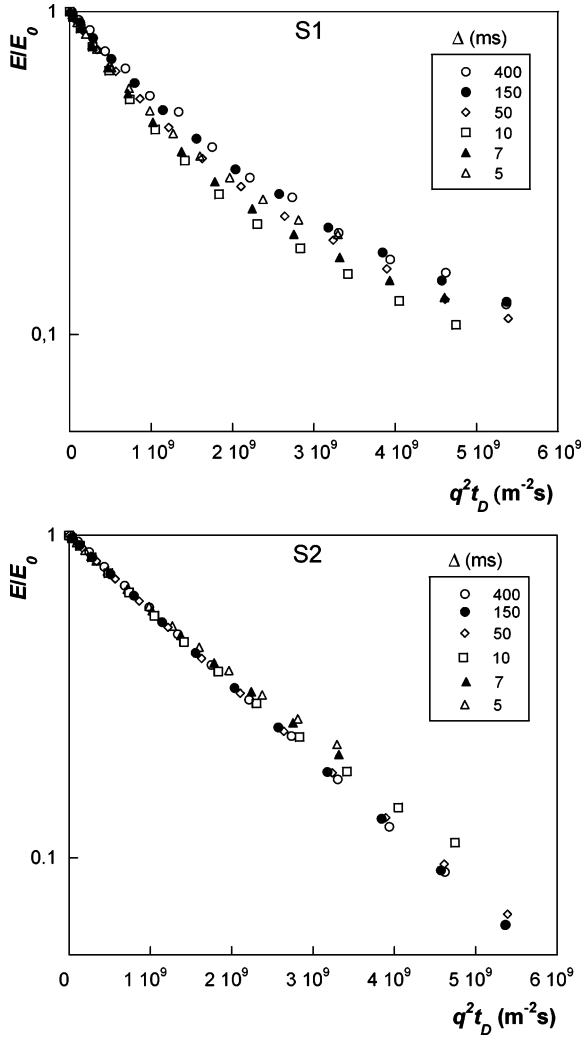

Figure 8. Semilog plot of the experimental water echo decay vs q^2t_D at different Δ values (sample S1: GTO/NaO/W = 30/30/40, sample S2: GTO/NaO/W = 20/20/60).

is not observed for sample S1, it can be inferred that water-restricted diffusion in sample S2 occurs in smaller domains. The latter remark is supported by the optical microscopy results, which indicate that sample S2 is characterized by smaller liposomes with respect to sample S1.

A problem of general interest for researchers involved in self-diffusion investigations is that of molecular transport within microscopic subregions.[18,19] If diffusion is unaffected by the boundaries between the individual subregions, the sample can be considered homogeneous. In the limiting case of completely restricted diffusion, molecules are confined within subregions and the signal is dependent on boundary conditions. For practical purposes, echo attenuation is approximated, in many cases, by a relation of the type in eq 2, with the true self-diffusion coefficient generally replaced by an apparent one. Measurements of the apparent self-diffusion coefficients as a function of time allow obtaining information about the tortuosity and permeability of complex systems.

The apparent water self-diffusion coefficients, D_D, of samples S1 and S2 were calculated for each Δ at small q^2t_D values. Results are shown in Figure 9.

In heterogeneous systems, the presence of dispersed particles reduces the volume available for diffusion thus affecting the self-diffusion coefficient observed (obstruction factor). Here,

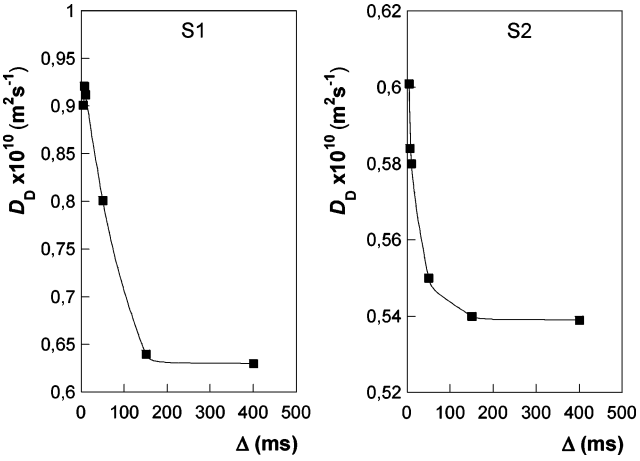

Figure 9. Water self-diffusion coefficients of the samples S1 and S2 determined at different Δ values (for sample composition see the text or Figure 8).

the obstruction to molecular motion is determined by the presence of both oil droplets and liposomes.

It has been shown[20] that the obstruction effect in systems containing spherical monodisperse particles (for other geometries similar equations can be derived) is given by

$$\frac{D_D}{D_0} = \frac{1}{1+\frac{\phi}{2}} \tag{12}$$

where D_D is the measured self-diffusion coefficient, D_0 is the self-diffusion coefficient of neat water, and ϕ is the volume fraction of the spheres. For $\phi = 50\%$ a value of 0.8 for the obstruction factor can be calculated. Because $D_0 = 1.872 \times 10^{-9}$ m^2 s^{-1}, this will give an effective self-diffusion coefficient of 1.456×10^{-9} m^2 s^{-1}. Thus, the very low values of the measured self-diffusion coefficients cannot be entirely attributed to an obstruction effect.

From data reported in Figure 9, it is worth stressing that the D_D time-dependent behavior is observed in both samples only for Δ < 150 ms. As to the inner structure of the system, we notice that a finite asymptotic limit of D_D at long diffusion times, $D_D(\infty)$, is indicative of a "connected porous system".[21] Tanner[22] showed that a heterogeneous connected porous system may be approximated by parallel planar barriers of equal but arbitrary permeability, p. By extrapolating from a plot of Figure 9 $D_D(t = 0) = D_0$, the reduced permeability $P = pa/D_0$ (where a is the constraint spacing) can be directly evaluated by

$$P = \frac{1}{\frac{D_0}{D_{w(\infty)}} - 1} \tag{13}$$

The time t^*, at which the diffusivity takes its long-term behavior, corresponding to $t^* \approx a^2/D_0$, can be estimated from plot of Figure 9 to be $t^* \approx 150$ ms. Since

$$P = pa/D_0 = p\sqrt{\frac{t^*}{D_0}} \tag{14}$$

it turns out that $p \approx 2 \times 10^{-2}$ cm s^{-1} and 4×10^{-2} cm s^{-1} are obtained for the samples S1 and S2, respectively. These values appear of the same order estimated in organic or biological systems.[23,24]

4. Conclusions

The GTO/NaO/W ternary system, here explored by optical microscopy and NMR methods, represents a fully biocompatible formulation useful in cosmetic, food and pharmaceutical applications. Several monophasic and biphasic regions where a lamellar phase coexists with different isotropic phases are identified. The wide emulsion region that extends from the center of the ternary diagram toward the water corner is characterized by the presence of small oil droplets dispersed into the lamellar phase. This should be of great interest in the formulation of drug delivery systems. Along with the capacity to host hydrophobic drugs, low energy input during the preparation stage and high stability are added values. In accordance with water NMR self-diffusion data, the occurrence of a connected porous structure of these heterogeneous samples is strongly suggested. On the contrary, oil molecules are forced to diffuse into spherical domains. Sizing of oil droplets within this emulsion region was provided through VEM at different storage times. A highly polydisperse log-normal distribution was proven. The negligible differences found in the droplets size distribution upon sample aging lead us to confirm the recognized stabilizing capacity against coalescence ascribed to the presence of the LC phase. It should be also highlighted that in this system the L_α phase represents the whole dispersing medium and not simply a protecting layer around the droplet. Therefore, also creaming processes should be greatly slowed down. Indeed, samples within the emulsion region stored at 25 °C did not show any macroscopic phase separation after several months from their preparation.

Acknowledgment. Consorzio Sistemi Grande Interfase (CSGI-Firenze) and MURST−PRIN 40% (Italy) are gratefully acknowledged for financial support.

References and Notes

(1) Caboi, F.; Murgia, S.; Monduzzi, M.; Lazzari, P. *Langmuir* **2002**, *18*, 7916.
(2) Collins-Gold, L.; Feichtinger, N.; Wärnheim, T. *Modern Drug Discovery* **2000**, *3*, 44.
(3) Mele, S.; Murgia, S.; Monduzzi, M. *Colloid Surf. A* **2003**, *228*, 57.
(4) Mele, S.; Murgia, S.; Monduzzi, M. *Langmuir* **2004**, *20*, 5241.
(5) Strickley, R. G. *Pharm. Res.* **2004**, *21*, 201.
(6) Hartshorne, N. H. *The Microscopy of Liquid Crystals*; Microscope Publications Ltd.: London, 1974.
(7) Abragam, A. *The Principle of Nuclear Magnetism*; Oxford University Press: New York, 1985.
(8) Lindblom, G.; Lindman, B.; Tiddy, G. J. T. *Acta. Chem. Scand. A* **1975**, *29*, 876.
(9) Kato, T.; Terao, T.; Tsukada, M.; Seimiya, T. *J. Phys. Chem.* **1993**, *97*, 3910.
(10) Callaghan, P. T. *Principles of Nuclear Magnetic Resonance Microscopy*; Clarendon Press: Oxford, 1991.
(11) Borné, J.; Nylander, T.; Khan, A. *Langmuir* **2001**, *17*, 7742.
(12) Lindblom, G.; Rilfors, L.; Hauksson, J. B.; Brentel, I.; Sjölund, M.; Bergenståhl, B. *Biochemistry* **1991**, *30*, 10938.
(13) Marques, E. F. *Langmuir* **2000**, *16*, 4798.
(14) Holstborg, J.; Pedersen, B. V.; Krog, N.; Olesen, S. K. *Colloid Surf. B* **1999**, *12*, 383.
(15) Pitzalis, P.; Monduzzi, M.; Krog, N.; Larsson, H.; Ljusberg Wahren, H.; Nylander, T. *Langmuir* **2000**, *16*, 6358.
(16) Ambrosone, L.; Colafemmina, G.; Palazzo, G.; Ceglie, A. *Prog. Polym. Sci.* **2000**, *115*, 161.
(17) Cichocki, B.; Felderhof, B. U. *Langmuir* **1992**, *8*, 2889.
(18) Kärger, J.; Pfeifer, H.; Heink, W. In *Advances in Magnetic Resonance*; Waugh, J. S., Ed.; Academic Press: San Diego, 1981; Vol. 12, p 1.
(19) Kärger, J.; Pfeifer, H. *Zeolites* **1987**, *6*, 90.
(20) Jönson, B.; Wennerström, H.; Nilsson, P. G.; Linse, P. *Colloid Polym. Sci.* **1986**, *264*, 77.
(21) Mitra, P. P.; Sen, P. N.; Schwartz, L. M.; Le Doussal, P. *Phys. Rev. Lett.* **1992**, *68*, 3555.
(22) Tanner, J. E. *J. Chem. Phys.* **1978**, *69*, 1748.
(23) Meerwall, Von E.; Ferguson, R. D. *J. Chem. Phys.* **1981**, *74*, 6965.
(24) Latour, L. L.; Svoboda, K.; Mitra P. P.; Sotak, C. H. *Proc. Natl. Acad. Sci. U.S.A.* **1994**, *91*, 1229.